Journal of Inflammation Research

Dovepress
Taylor & Francis Group

Open Access Full Text Article

ORIGINAL RESEARCH

Si-Ni Decoction as a Potential Treatment for Ulcerative Colitis: Modulation of Gut Microbiota and AKT1 Inhibition Through Network Pharmacology and in vivo Validation

Lihao Shi[1], Leilei Chen[1], Guiyuan Jin[2], Yonghong Yang[2], Fengqin Zhu[3], Guangxi Zhou[1,3]

[1]Cheeloo College of Medicine, Shandong University, Jinan, People's Republic of China; [2]Medical Research Center, Affiliated Hospital of Jining Medical University, Jining, People's Republic of China; [3]Department of Gastroenterology, Affiliated Hospital of Jining Medical University, Jining, People's Republic of China

Correspondence: Guangxi Zhou, Cheeloo College of Medicine, Shandong University, Jinan, People's Republic of China, Tel +86 0537-2903975, Email zgx_viola@126.com

Background: Sini Decoction (SND), a time-honored formulation in traditional Chinese medicine, consists of three key ingredients: aconite, licorice, and ginger rhizome. It has been used for more than a thousand years to relieve symptoms associated with acute gastroenteritis, dyspepsia, and abdominal discomfort, but its therapeutic efficacy in ulcerative colitis (UC) and the mechanisms involved have not been validated. In this study, a comprehensive approach integrating network pharmacology, molecular docking, molecular dynamics simulation and experimentation was used to assess the efficacy of SND in the treatment of UC and to explore its molecular mechanisms.

Methods: The bioactive compounds associated with ulcerative colitis (UC) were identified using the TCMSP database, with potential targets predicted via the Swiss Target Prediction database. Protein-protein interaction networks were constructed using the STRING database and Cytoscape and the most important genes were identified. Subsequently, molecular docking was combined with molecular dynamics simulations using molecular docking to assess the binding affinity of the main active ingredient of SND to AKT1. To evaluate the therapeutic effects of SND, we utilized a dextran sodium sulfate-induced UC mouse model. Additionally, fecal samples were collected for analysis of the intestinal microbiota to explore the influence of SND on gut flora composition.

Results: Fifteen bioactive components from SND were identified, and their activities were validated. The results indicated that AKT serine/threonine kinase 1 is a core target of SND for the treatment of UC. The anti-inflammatory, intestinal barrier-protective, and microbiota-regulating effects of SND were confirmed in animal models, alongside evidence of its inhibitory effect on AKT1.

Conclusion: The active ingredients of SND were screened, with a focus on AKT1 inhibition, to reduce inflammation in UC, protect the intestinal barrier, and regulate the intestinal microbiota, demonstrating significant therapeutic potential.

Keywords: sini decoction, ulcerative colitis, network pharmacology, gut microbiota, intestinal barrier, molecular docking

Introduction

Ulcerative colitis (UC), a chronic inflammatory condition, primarily affecting the colon and rectum. The hallmark of UC is persistent inflammation of the mucosal lining, often accompanied by disruption of the intestinal barrier and dysbiosis in the gut microbiota.[1] Although the exact cause of UC remains unknown, current research points to a multifactorial etiology,[2] involving genetic predisposition,[3] environmental influences such as diet and lifestyle,[4] and alterations in the gut microbiota.[2]

Patients with UC commonly experience gastrointestinal symptoms, including abdominal pain, diarrhea, and muco-purulent blood in the stools, often accompanied by disrupted bowel habits,[5] leading to damage to the colonic mucosal barrier and disruption of the intestinal microbiota.[6] The mucosal epithelium serves as the gut's natural protective barrier,

Received: 27 January 2025
Accepted: 26 April 2025
Published: 14 May 2025

preventing pathogenic antigens, such as bacteria, from penetrating the mucosal layer.[7] When the intestinal barrier is compromised, it leads to disturbances in the intestinal flora, manifested by a decrease in beneficial microorganisms, as well as an increase in pathogenic bacteria.[7,8] With advancing understanding of UC, the current therapeutic approach aims to simultaneously alleviate inflammation, repair the mucosal barrier, and regulate the intestinal microbiota. This strategy not only reduces reliance on hormonal treatments and surgery but also significantly improves long-term prognosis and enhances patients' quality of life.[9]

AKT serine/threonine kinase 1 (AKT1) is an enzyme critical to various cellular processes, including the regulation of immune responses, intestinal barrier function, and inflammation in the gut. Consequently, signaling pathways that modulate these functions are likely pivotal in the pathogenesis of UC.[10–12]

Sini Decoction (SND), a time-honored formulation in traditional Chinese medicine, consists of three key ingredients: aconite, licorice, and ginger rhizome. It has been officially recognized in the 2020 edition of the Chinese Pharmacopoeia,[13] For more than a thousand years, it has been used to treat various causes of acute gastroenteritis or indigestion and abdominal pain. SND has demonstrated notable anti-inflammatory effects and has been used successfully to reverse shock in patients and animal models of severe infection.[13–16] However, research on the potential benefits of SND in ulcerative colitis is limited. Elucidating its therapeutic role and mechanisms could help incorporate SND into precision medicine strategies for UC.

This study aimed to evaluate the anti-colitis effects of SND from multiple perspectives, investigating its main active ingredients and targets. Through network pharmacology, molecular docking, and molecular dynamics simulations, complemented by experimental data, the study seeks to elucidate the role of SND in the treatment of UC.

Materials and Methods

Active Ingredients of SND and Target Prediction

The active compounds of SND were identified the TCMSP Database and Analysis Platform (https://old.tcmsp-e.com/tcmsp.php). Compounds related to "aconite", "licorice", and "ginger rhizome" were searched, compounds were determined to be active only when oral bioavailability was ≥ 30% and drug similarity was ≥ 0.18%.[17] After identifying the active compounds, their potential target proteins were predicted using the STRING database (http://www.string-db.org), and target protein names were converted to their corresponding gene symbols for further analysis.[18]

Screening of UC-Related Targets

Using "Ulcerative Colitis" as the search term, disease-related targets were identified through the DisGeNET database (http://www.disgenet.org) and GeneCards (https://www.genecards.org/).[19]

Network Pharmacology

Predicting potential anti-UC targets of SND using a bioinformatics online platform (http://www.bioinformat-ics.com.cn).[20] GO and KEGG enrichment analyses of key target genes were performed using Metascape (https://metascape.org/gp) and DisGeNET databases, and Sankey diagrams were created using the Bioinformatics Online platform (https://www.bioinformatics.com.cn) to visualize these relationships.[21] STRING database to perform the next step in the analysis, the minimum interaction score was set to 0.40 to ensure high confidence. A Protein-Protein Interaction (PPI) Network was generated to identify the most important genes using Cytoscape (3.8.0, Oracle, USA) as well as the cytoHubba plugin. Herbs, active compounds of SND and UC-related targets were used to construct network diagrams to visualize the relationship between these elements by Cytoscape.[22]

Molecular Docking

The 2D structure of the small molecule ligand was retrieved from the PubChem database (http://pubchem.ncbi.nlm.nih.gov/) and converted into a 3D structure using ChemOffice software, then saved as a mol2 file. The RCSB PDB database (http://www.rcsb.org/) was used to select a high-resolution crystal structure of the protein target as the receptor. The protein was then dehydrogenated and dephosphorylated using PyMOL software and saved as

a PDB file. Molecular docking was conducted using AutoDock Vina 1.5.6 software to explore protein-ligand interactions. The structure of proteins as well as small molecules were processed using Autodock to hydrogenate and dehydrate proteins, hydrogenate small molecule ligands, determine torsion force, etc., after which the coordinates of docking boxes were determined, and the optimal conformation of the molecular simulation was ultimately obtained by comparing the magnitude of scores of the docking results. Discovery Studio 2019 software was used to visualize 2D and 3D plots of the interactions between the test compounds and key residues. Binding energy (kcal/mol) < -5.0 indicates good binding activity, < -7.0 suggests strong binding activity.

Molecular Dynamics Simulation

MD simulations of the complexes were run for 100 ns with Gromacs 2023. The CHARMM 36[23] force field modeled the protein, and GAFF2 was used for the ligand. The complexes were placed in cubic boxes with periodic boundaries, and TIP3P water was added.[24] Electrostatic interactions were handled by PME, and integration used the Verlet algorithm. The system underwent 100,000 equilibration steps (isothermal-isovolumetric and isothermal-isobaric phases, coupling constant 0.1 ps, duration 100 ps). Van der Waals and Coulomb interactions had a 1.0 nm cutoff. Simulations were done at 300 K and 1 bar for 100 ns.

The Sini Decoction Preparation

The Sini decoction was made using finished drug (031439) purchased from KO DA Pharmaceuticals Ltd. in compliance with the marketing standards.

Dosage Information / Dosage Regimen

The Human Equivalent Dose (mg/kg) was calculated using the formula: Animal Dose (mg/kg) / Conversion Factor. Based on the manufacturer's instructions, the adult dose of 12 grams per day was converted to a mouse dose of 0.4065 mg per day.

Construction of a Mouse Model of Experimental Colitis and Treatment of SND

Mice were maintained in specific pathogen-free environments, with access to filtered air, sterile water, and autoclaved food. The male mice utilized in the experiments were aged 8 weeks and weighed between 20 and 23 grams. Mice were reared for 7 days with 2% dextrose sodium sulphate (DSS, MP Biomedicals) to construct an ulcerative colitis model, while SND was administered by gavage for 7 days. 60 mice were randomly allocated according to the number of mice in a group of 15 mice each.: control (Ctrl), SND control (SND Ctrl), DSS, and SND-treated DSS (SND DSS). For 10 days, the following indicators of acute colitis were assessed daily: diarrhea, presence of blood in stools, body weight, and survival rates. On the 10th day, fecal samples were collected, all mice were euthanized, and colonic tissues were harvested.

Quantitative Reverse Transcription-Polymerase Chain Reaction

RNA was extracted with Trizol (Invitrogen) and reverse transcribed to cDNA using the 5x All-In-One RT MasterMix kit (abm). qRT-PCR was performed with ChamQ SYBR qPCR Master Mix (Vazyme) following the manufacturer's protocol. mRNA levels were quantified with SYBR Green dye and analyzed by the 2-ΔΔCt method. β-actin served as the reference gene for normalization.

Hematoxylin and Eosin (H&E) Staining

Mouse colon samples were fixed in paraformaldehyde (PFA) for 48 hours. After fixation, the tissues were embedded in paraffin, sectioned into thin slices, and subjected to hematoxylin and eosin staining for histological examination.

Enzyme-Linked Immunosorbent Assay (ELISA)

Colonic tissue homogenates were prepared from the mice, and cytokine levels were quantified using enzyme-linked immunosorbent assay (ELISA) kits (JONLNBIO). Cytokines measured included IL-10 (sensitivity: 1.45 pg/mL, range: 3.12–200 pg/mL) and IL-1β (sensitivity: 2.9 pg/mL, range: 6.25–400 pg/mL).

Fecal Microbiota Analysis by 16S rRNA Sequencing

A fecal microbiota analysis was done via 16S rRNA sequencing. Mouse stool samples were collected before euthanasia and frozen in liquid nitrogen. Genomic DNA was extracted from 50–100 mg of feces using the TIANamp stool DNA kit. (TIANGEN Biotech, China). DNA concentration and purity were measured with a NanoDrop 2000C spectrophotometer (Thermo Fisher Scientific, USA). The 16S rRNA gene was amplified by PCR, and sequencing was performed on an Illumina MiSeq PE300 platform. (OE Biotech Co., Ltd).

Western Blotting

Tissue samples were lysed using RIPA assay buffer and evaluated for protein concentration using the BCA assay. The proteins were subsequently separated by SDS-PAGE and transferred onto PVDF membranes. To minimize non-specific binding, the membranes were treated with a blocking solution containing 3% BSAand incubated with primary antibodies at 4°C for 24 hours: anti-t-AkT1 (1:1000; ab314110; Abcam), anti-p-AkT1 (1:1000; ab223849; Abcam), and anti-β-actin (1:1000; AA128; Abcam). Following this, the membrane was incubated with HRP-conjugated secondary antibodies (1:3000; Beyotime) for 2 hours at room temperature. Protein bands were detected using enhanced chemiluminescence (Biosharp), and the membrane was visualized with the FluorChem E system (ProteinSimple). Results were normalized to β-actin levels as an internal control.

Immunofluorescence

Colon tissues from mice were collected, fixed in 4% paraformaldehyde, embedded in paraffin, and sectioned into 5-μm slices, which were mounted on glass slides for further analysis. After deparaffinization and rehydration, the tissue sections were incubated overnight at 4°C with primary antibodies: anti-E-cadherin (1:100, ab231303, Abcam), anti-Claudin-1 (1:100, ab307692, Abcam), anti-ZO-1 (1:100, ab190085, Abcam), and anti-occludin (1:250, ab216327, Abcam). After this incubation, the samples were protected from light and incubated at room temperature with anti-rabbit IgG-Alexa Fluor® 488 Conjugate (Proteintech, 1:500 dilution). Finally, DAPI was applied.

Permeability of FITC-Dextran

Mice were subjected to a fasting period of 12 hours prior to dissection and were administered 50 mg/kg of FITC-dextran orally. Four hours later, peripheral blood was collected from the mice and centrifuged at 3000 rpm for 10 minutes at 4°C. From the resulting supernatant, 100 μL of serum was extracted and placed in a 96-well plate. The fluorescence intensity of the serum was evaluated using a fluorescence microplate reader with an excitation wavelength of 480 nm and an emission wavelength of 520 nm.

Statistical Analysis

The results are presented as mean ± standard deviation. Statistical analyses were performed using GraphPad Prism 8. Comparisons between two or more groups were made using two-tailed Student's *t*-tests or one-way analysis of variance (ANOVA) followed by a Bonferroni post-test. A p-value of less than 0.05 was considered statistically significant.

Results

Predicting the Therapeutic Components of Sini Decoction

Sini decoction was found to share 193 potential targets with 1,127 genes relevant to colitis (Figure 1A). Following our previously described method, we obtained 10,85,3 active active ingredients from "aconite", "licorice", and "ginger rhizome", respectively (Supplementary data 1), and then imported the herbs, SND active compounds, and UC-related targets into the Cytoscape software to draw herb-compound-target-network diagrams (Figure 1B). Topologically, the most critical nodes in this network were determined based on three key metrics: betweenness centrality, degree, and closeness centrality. The "degree" of a node refers to the number of connections (edges) it has, "betweenness" measures how many of the shortest path's pass through a node, and "closeness" reflects the average distance from one node to all others in the network. We have

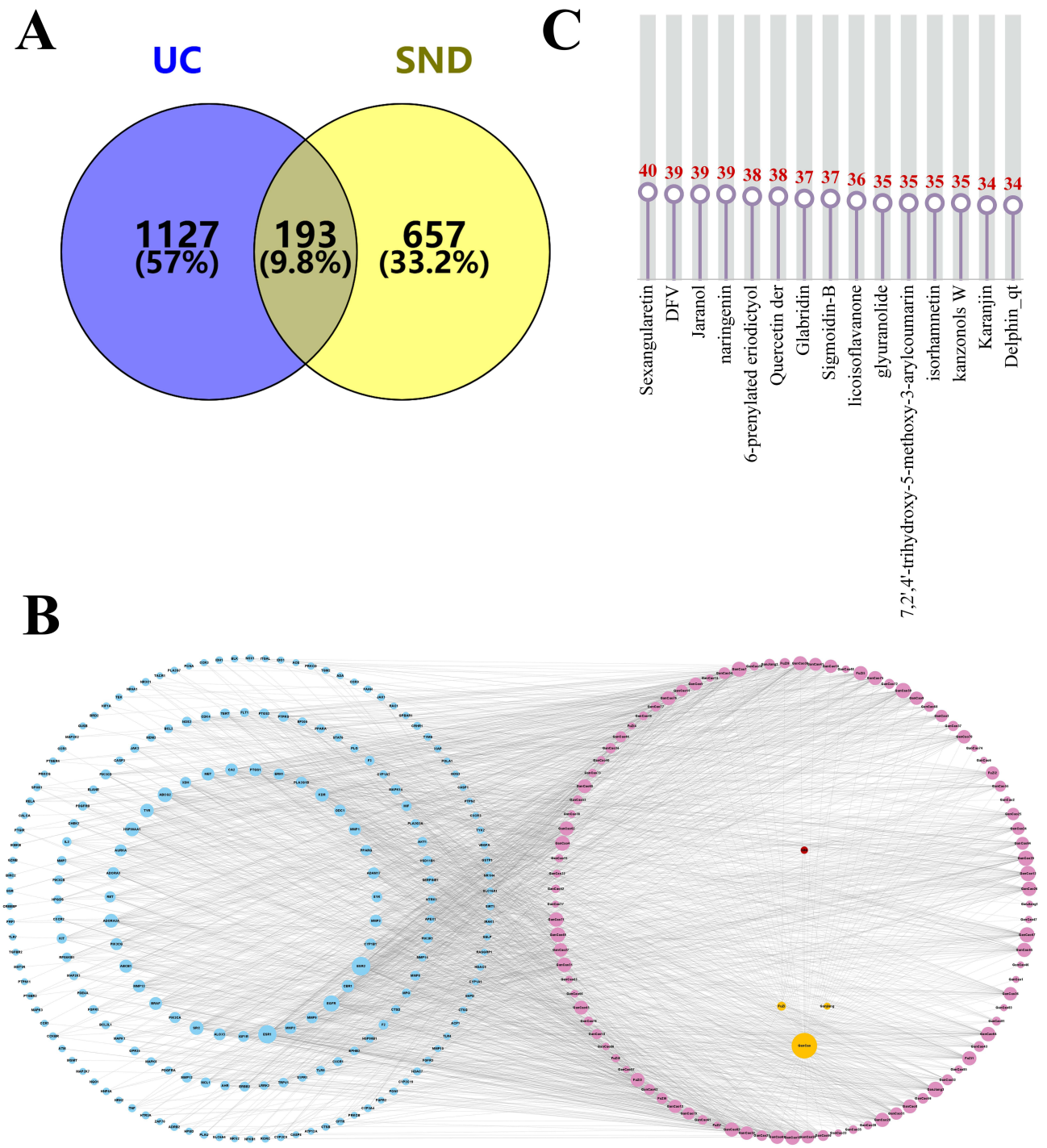

Figure 1 Screening of SND targets and key active ingredients for the treatment of UC. (**A**) Venn diagram, illustrating a total of 193 overlapping genes associated with ulcerative colitis in SND treatment. (**B**) Herbs- Compounds-Target Network Construction of SND in the treatment of UC. (**C**) All active ingredients were ranked according to "degree" and the top 15 active compounds were selected.

ranked all active ingredients by "degree" and selected the top 15 active compounds (Figure 1C). A total of one of these fifteen compounds is from "ginger rhizome", two are from "aconite", and twelve are from "licorice", whose specific information is presented in Table 1, and whose specific chemical expressions can be found at Figure 2

https://doi.org/10.2147/JIR.S516556

Table 1 Top 15 Active Compounds

Source	Mol ID	Molecule Name	Degree	Betweenness	Closeness
Ginger rhizome	MOL002514	Sexangularetin	40.0	1277.038	0.40358126
Licorice	MOL001792	DFV	39.0	2274.856	0.41267607
Licorice	MOL000239	Jaranol	39.0	1579.5206	0.4138418
Licorice	MOL004328	naringenin	39.0	1887.025	0.41267607
Licorice	MOL004989	6-prenylated eriodictyol	38.0	1799.2715	0.41267607
Licorice	MOL004961	Quercetin der	38.0	1062.9915	0.41267607
Licorice	MOL004908	Glabridin	37.0	1995.9838	0.41151685
Licorice	MOL004935	Sigmoidin-B	37.0	1183.2141	0.41036415
Licorice	MOL004885	licoisoflavanone	36.0	2452.42	0.41036415
Licorice	MOL004905	glyuranolide	35.0	3912.0627	0.40807799
Licorice	MOL004990	7,2',4'-trihydroxy–5-methoxy-3–arylcoumarin	35.0	1085.7054	0.40921786
Licorice	MOL000354	isorhamnetin	35.0	816.4049	0.40921786
Licorice	MOL004820	kanzonols W	35.0	1915.6273	0.40807799
Aconite	MOL002398	Karanjin	34.0	2213.0786	0.3980978
Aconite	MOL002388	Delphin_qt	34.0	995.2379	0.39381722

Notes: The "Mol ID" is information derived from the drug defined in the TCMSP; The "degree" of a node refers to the number of connections (edges) it has, "betweenness" measures how many of the shortest path's pass through a node, and "closeness" reflects the average distance from one node to all others in the network.

Screening and Visual Network Analysis of Potential SND Targets for the Treatment of UC

A PPI network for herb-compound and disease-target interactions was constructed using the STRING database, with a confidence score threshold of 0.4 or higher. This network included 193 nodes and 3479 edges, with an average node

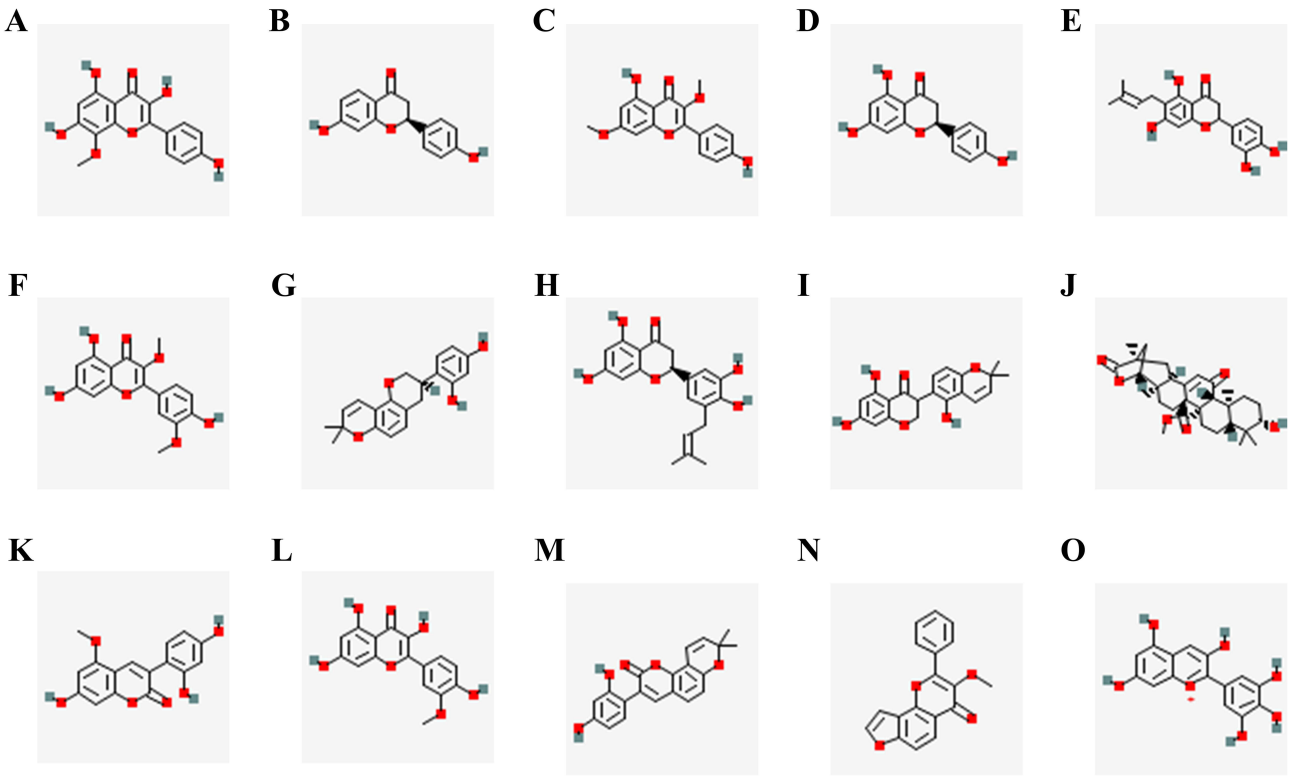

Figure 2 Specific chemical formulae for the first 15 active compounds. From (**A**–**O**) are Sexangularetin, DFV, Jaranol.naringenin.6-prenylated eriodictyol, Quercetin der., Glabridin, Sigmoidin-B, licoisoflavanone, glyuranolide, 7,2',4'-trihydroxy–5-methoxy-3–arylcoumarin, isorhamnetin, kanzonols W, Karanjin, Delphin_qt. Protein-protein interaction (PPI) network depicting the interactions of SND-related proteins involved in UC treatment.

degree of 36.1 and a local clustering coefficient of 0.57 (Figure 3A). Under Cytoscape (CytoHubba plug-in) analysis, the first 32 key genes were identified according to their degree, betweenness, and closeness centrality (closeness > 0.00279, betweenness > 171.82383, degree > 36.05181) (Figure 3B). Among them, we visualised and analysed these 32 core targets. The most prominent hub gene obtained was AKT1 (Figure 3C).

GO Enrichment Analysis

GO enrichment analysis of potential target genes using the DAVID database, covering three categories: Biological Process (BP), Cellular Component (CC), and Molecular Function (MF) (Figure 4A). The top 10 enriched BP terms included processes such as positive regulation of protein phosphorylation, inflammatory response, and phosphorylation. The top 10 enriched MF terms were primarily associated with protein tyrosine kinase activity, protein kinase activity, and enzyme binding. Similarly, the top 10 enriched CC terms are also shown.

KEGG Enrichment Analysis

Overlapping genes of the KEGG signaling pathway were enriched using the Metascape database. Top KEGG pathways A total of 20 were identified, included key pathways related to cancer, positive regulation of cell motility, response to bacterial molecules, regulation of phosphorus metabolism, signaling by interleukins, and the gastrin signaling pathway (Figure 4B).

Molecular Docking and Molecular Dynamics Simulation

We molecularly docked 15 previously mined active compounds with AKT1 protein (Supplementary data 2) to further explore the downstream mechanism of SND for UC. The results showed that all 15 compounds had meaningful binding activity to AKT1 below −5.0 kcal/mol, and we selected 10 compounds below −6.0 kcal/mol for our visualisation and analysis by Discovery Studio 2019, namely Delphin_qt from "aconite", DFV, Quercetin der, licoisoflavanone, Jaranol,6-prenylated eriodictyol,7,2',4'-trihydroxy-5-methoxy-3-arylcoumarin, Glabridin, kanzonols W from "licorice"and Sexangularetin from "ginger rhizome" (Figure 5). We finally selected the compound with the lowest binding affinity among the three herbal components of SND (Quercetin der, Delphin_gt, Sexangularetin) for simulating molecular dynamics. RMSD measures the conformational stability of proteins and ligands, indicating how much atomic positions deviate from their initial positions. The smaller the deviation, the better the conformational stability. Therefore, the equilibrium of the simulation system was evaluated using RMSD. As shown in (Figure 6A), the AKT1-Delphin complex system fluctuates steadily between 10ns-60ns, showing a slight upward trend after 60ns but overall fluctuating below 2.8 Å. The AKT1-Quercetin complex system reaches equilibrium after 85ns and finally fluctuates around 4.1 Å. The AKT1-Sexangularetin complex system reaches equilibrium after 10ns and finally fluctuates around 3.1Å. Therefore, the 3 small molecules showed high stability when binding to AKT1 target proteins. AND the radius of gyration (Rg) values of AKT1-Delphin, AKT1-Quercetin and AKT1-Sexangularetin complex systems showed slight fluctuations with solvent-accessible surface area (SASA) during the movement. It indicates that the AKT1-Delphin, AKT1-Quercetin and AKT1-Sexangularetin complex systems underwent conformational changes during motions (Figure 6B and C). The number of hydrogen bonds between the AKT1-Delphin complex system ranges from 0 to 9. In most cases, the complexes have about 6 hydrogen bonds. The number of hydrogen bonds between the AKT1-Quercetin der complex system ranges from 0 to 4. In most cases, the complexes have about 3 hydrogen bonds. The number of hydrogen bonds between AKT1-Sexangularetin complex systems ranged from 0 to 6. In most cases, the complexes had approximately 4 hydrogen bonds, suggesting that Delphin, Sexangularetin, and Quercetin der small molecules have good hydrogen bonding interactions with AKT1 target proteins (Figure 6D).

RMSF indicates the flexibility of amino acid residues in proteins. As shown in (Figure 6E), the AKT1-Delphin, AKT1-Quercetin der and AKT1-Sexangularetin complex systems have relatively low RMSF values (mostly below 4 Å), which makes them less flexible and more stable In summary, the AKT1-Delphin, AKT1-Quercetin der and AKT1-Sexangularetin complex systems are binding stable.

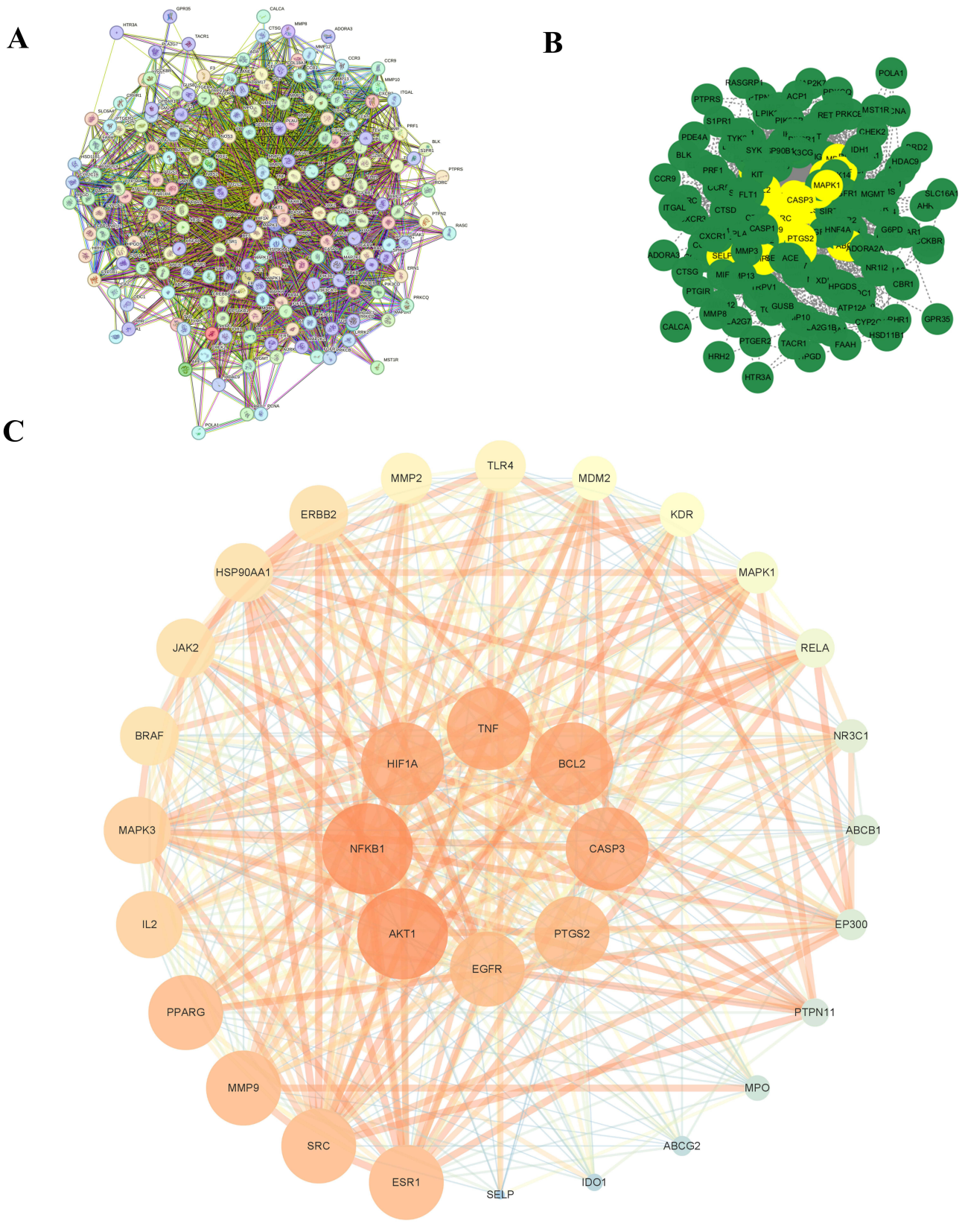

Figure 3 PPI network of SND targets in UC therapy and core targets. (**A**) PPI network of 193 targets in the STRING database. (**B**) 32 core targets were screened out of the 193 individual targets, where the core targets were labelled in yellow. (**C**) The PPI network was analysed using the Cytoscape software to analyse the PPI network to show the key targets affected by CR. The higher the degree value, the closer the colour is to red.

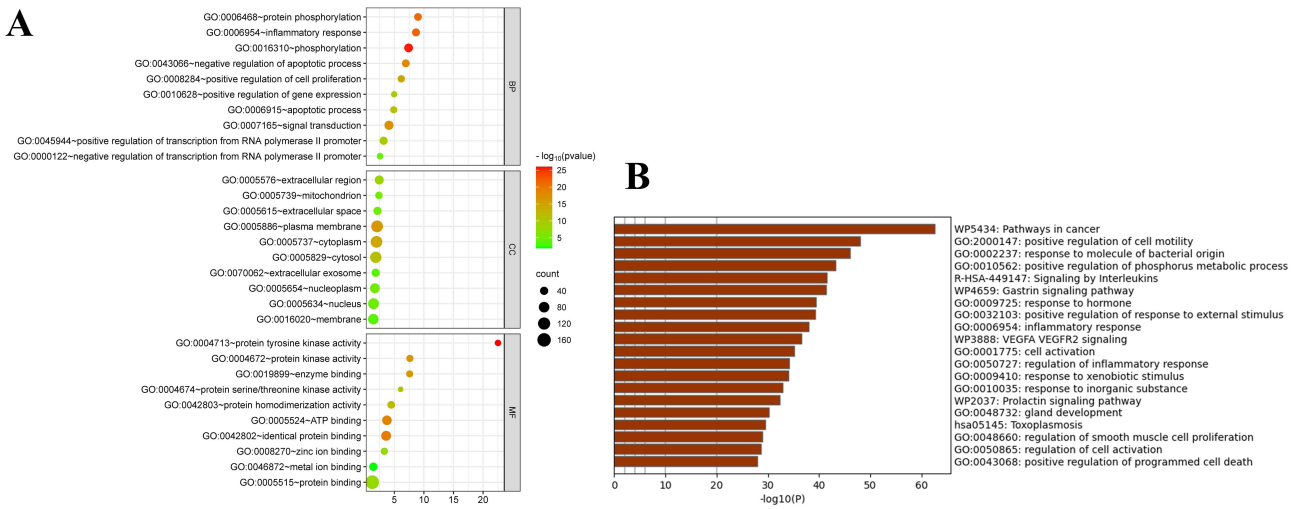

Figure 4 GO and KEGG enrichment analysis of the target of OA treated by CR. (**A**) GO analysis was performed to predict biological processes/cellular components/molecular functions affected by SND. The horizontal axis as well as the large of the dots indicate the number of small, enriched genes, the closer the colour to red means the closer the P-value is to zero, and the vertical axis indicates the name of the term. (**B**) KEGG analysis was performed to predict pathways affected by snd. The horizontal axis is the number of genes, and the vertical axis is the term name.

Therapeutic Effect of Sini Decoction on UC

DSS significantly reduced colon length in mice, an effect that was markedly reversed by SND (Figure 7A and B). SND also mitigated the severe weight loss and improved the DAI score in colitis mice (Figure 7C and D). Similarly, H&E stained photographs showed that SND reduced the histological changes caused by colitis this is consistent with macroscopic changes in the colon. (Figure 7E).

SND Suppresses Inflammation

We found that SND inhibited the increase in IL-1β levels in colon tissue homogenates of DSS mice and suppressed the decrease in IL-10 levels. (Figure 8A and B). In addition, SND reduced the mRNA expression levels of IL-Iβ, IL-6, TNF-α, and IL-17A in colon samples from mice with colitis and suppressed the decrease in IL-10 mRNA expression levels (Figure 8C–G). Next, we examined the protein expression of AKT and p-AKT by Western blotting. The expression of p-AKT was significantly increased in the DSS group (Figure 8H). In contrast, it was suppressed in the SND DSS group, which verified our findings through network pharmacology that SND inhibits the AKT pathway.

SND Alleviates the Impaired Intestinal Barrier Associated with Colitis

We used immunofluorescence to assess the integrity of tight junction proteins in the intestine, specifically Occludin, E-cadherin, Claudin- 1, and ZO-1. Our results showed that the expression of these tight junction proteins was significantly increased in the SND-treated DSS group compared to the DSS-only group (Figure 9A). To further confirm the therapeutic effect of SND, we gavage the four groups of mice with FITC-Dextran and measured fluorescence levels in their plasma. Consistently, SND treatment effectively alleviated intestinal barrier breakdown caused by colitis (Figure 9B).

SND Treatment Alters Microbiota Composition in Mice

Collecting the faeces from each group of mice and analyzing the composition of their flora, we found that the intestinal flora of the mice was altered after treatment with SND, most notably in the β-diversity, as can be well demonstrated by the UPGMA sample-level clustering plot (Figure 10A), PCA and PCoA analyses also demonstrated alterations in β-diversity following SND treatment (Figure 10B and C).

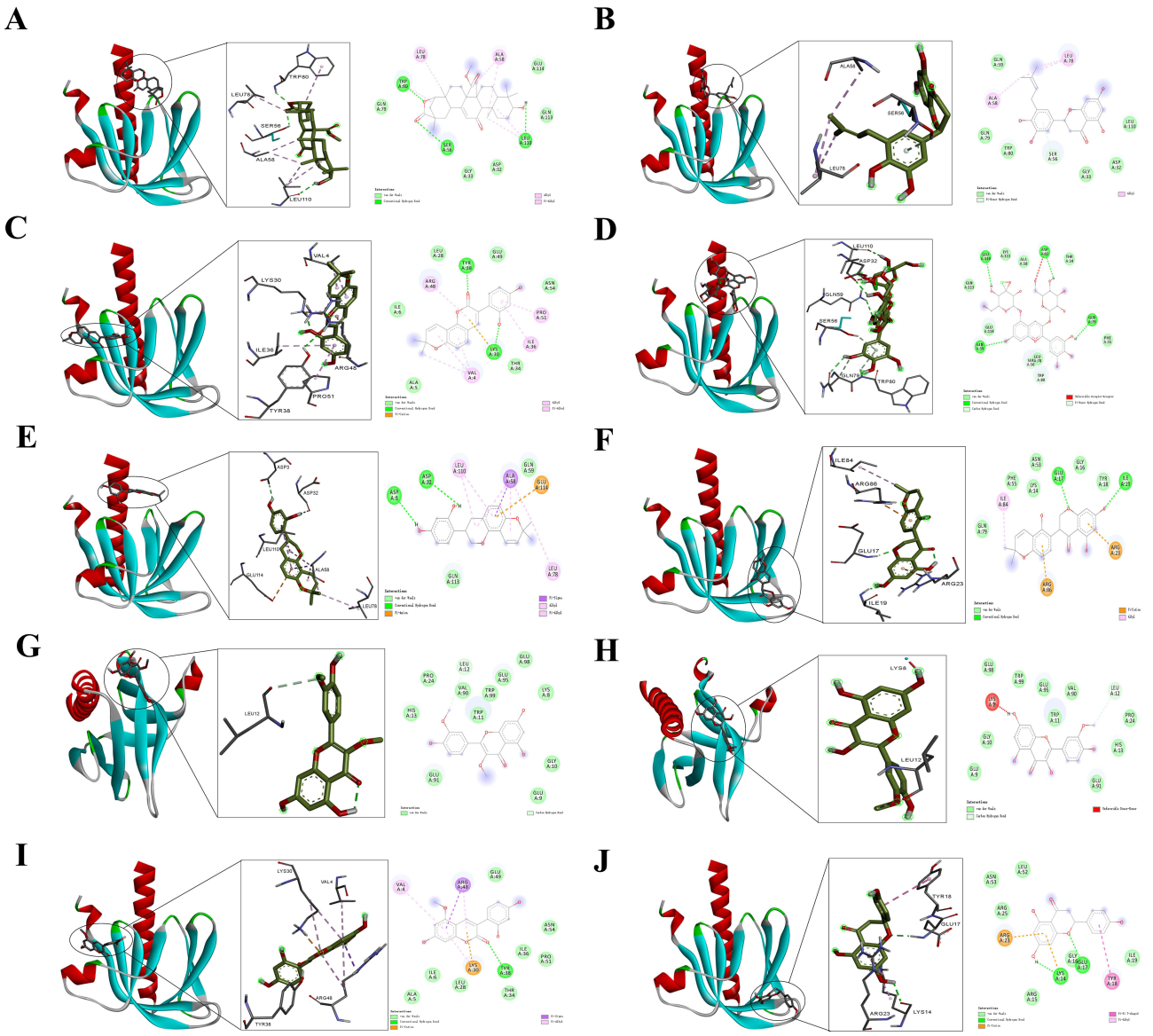

Figure 5 Molecular docking of key components of SND and AKT1. From (**A–J**) are Q Quercetin der., Delphin_qt, licoisoflavanone, Jaranol, 6-prenylated eriodictyol, 7,2',4'-trihydroxy–5-methoxy-3–arylcoumarin, Glabridin, kanzonols W, Sexangularetin, DFV.

SND Increased Beneficial Bacteria and Decreased Harmful Bacteria

Histograms of the relative abundance for the top 15 species at the phylum (Figure 11A), order (Figure 11D), and family levels (Figure 11G) illustrate differences in microbial composition among groups following SND treatment. At the phylum level, Desulfobacterota levels were significantly increased in DSS-treated mice compared to non-DSS-treated controls (Figure 11B). However, the increase was less pronounced in the SND-treated DSS group than in the DSS-only group. In contrast, Bacteroidota levels (Figure 11C) were markedly reduced in the DSS group but were restored by SND treatment. At the order level, Desulfovibrionales levels were significantly elevated in DSS-treated mice relative to controls (Figure 11E), but the elevation was smaller in SND-treated DSS mice compared to the DSS-only group. Conversely, Lactobacillales levels (Figure 11F) were significantly decreased in the DSS group, and this reduction was reversed with SND treatment. At the family level, Desulfovibrionaceae levels were significantly higher in DSS-treated mice compared to controls (Figure 11H), but the increase was less pronounced in SND-treated DSS mice than in the DSS-only group. Similarly, Peptococcaceae levels (Figure 11I) were substantially reduced in the DSS group, but SND treatment restored them.

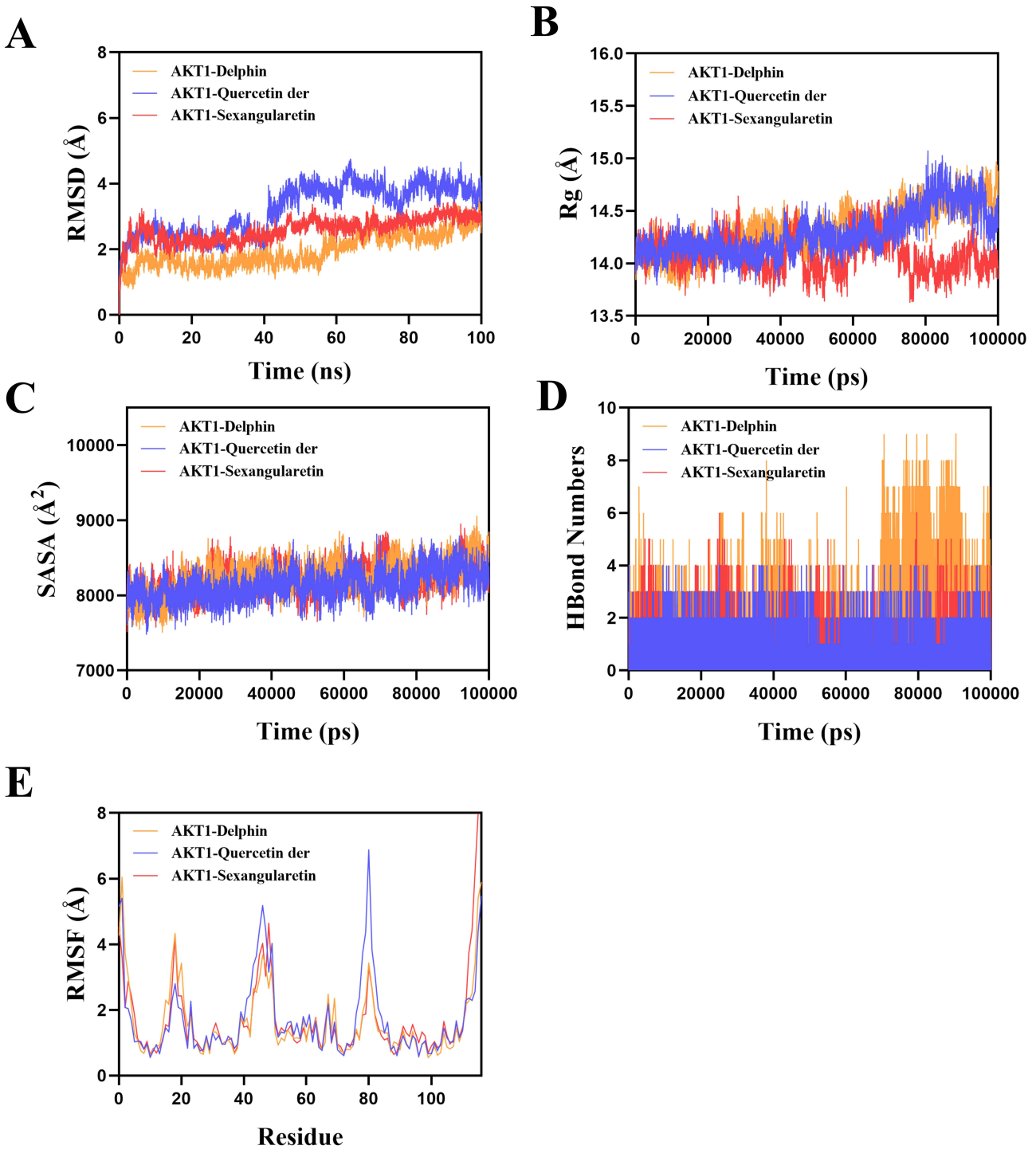

Figure 6 Molecular dynamics modelling of three herbal components of SND (Quercetin der, Delphin_gt and Sexangularetin). **A** The root mean square deviation (RMSD) of AKT1-Delphin complex system, AKT1-Quercetin complex system, and AKT1-Sexangularetin complex system, the smaller the deviation, the better the conformational stability. **B-C** Radius of Gyration (Rg) and solvent-accessible surface area (SASA) of AKT1-Delphin, AKT1-Quercetin and AKT1-Sexangularetin composite systems, the slight fluctuation of the complex during movement indicates that the complex system has undergone conformational changes during movement. **D** The number of hydrogen bonds between small molecules and target proteins in the kinetic process, and the number of hydrogen bonds between AKT1-Delphin complex systems ranged from 0 to 9. In most cases, the complex has about six hydrogen bonds. The number of hydrogen bonds between the AKT1-Quercetin der complex systems ranges from 0 to 4. In most cases, the complex has about three hydrogen bonds. The number of hydrogen bonds between the AKT1-Sexangularetin complex systems ranges from 0 to 6. In most cases, the complex has about four hydrogen bonds. **E** Root mean square fluctuation (RMSF) of AKT1-Delphin, AKT1-Quercetin der and AKT1-Sexangularetin complex Systems.

https://doi.org/10.2147/JIR.S516556

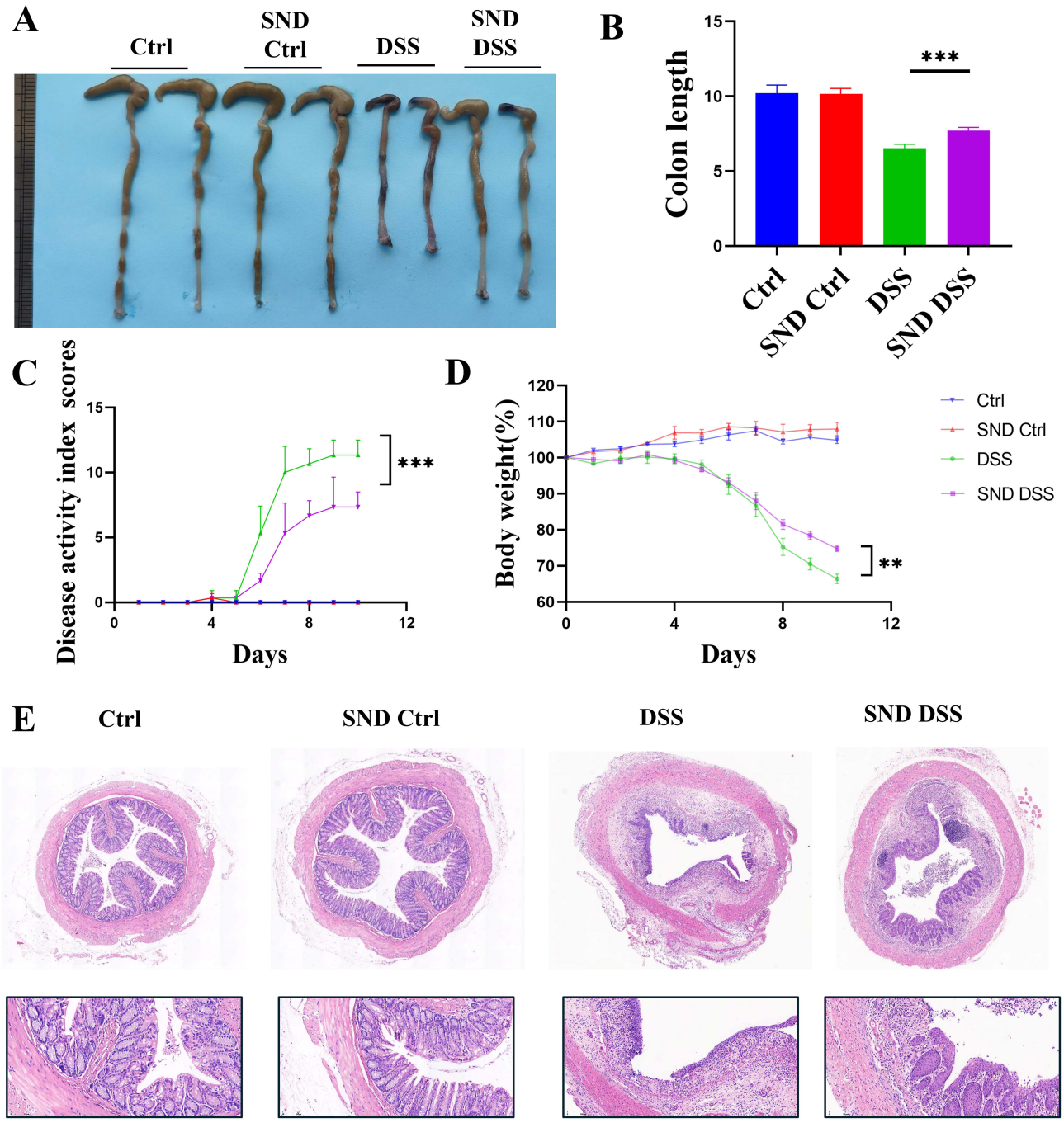

Figure 7 SND suppresses the progression of experimental colitis. To induce colitis in mice, mice were first treated with 2% DSS for 7 days, while SND was gavage for 7 days, and mice received 0.9% saline as a negative control. (**A**) Representative mouse gross morphology of the colon images was captured. (**B**) Colon length was measured. (**C**) DAI of mice was calculated daily during the period of observation. (**D**) The changes of body weight of mice were expressed as a percentage of the initial weight at the start of the experiment. (**E**) Representative photomicrographs of colon sections stained with haematoxylin and eosin (H&E) were examined. $^{**}P < 0.01$, $^{***}P < 0.001$.

Discussion

SND significantly reduced the development and severity of experimental colitis in mice, as demonstrated in our mouse colitis model using 2% DSS. This was evidenced by improved colon length, reduced weight loss, and lower DAI scores

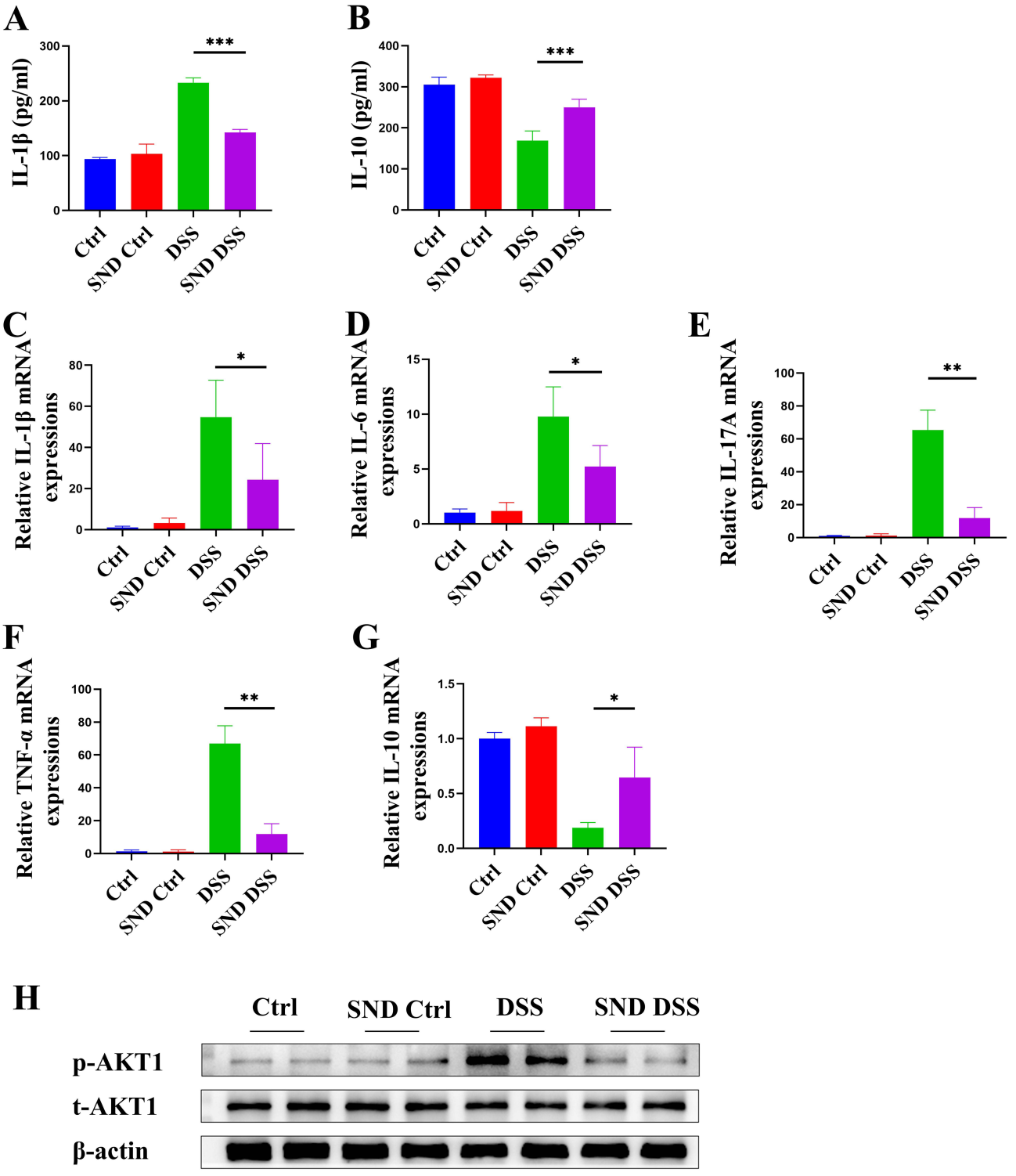

Figure 8 SND treatment inhibits the expression of pro-inflammatory genes and promotes the expression of anti-inflammatory genes in DSS-induced colitis in mice. (**A**) SND inhibited the increase in IL-1β levels in colon tissue homogenates of DSS mice and (**B**) suppressed the decrease in IL-10 levels. (**C**–**F**) SND reduced the mRNA expression levels of IL-Iβ, IL-6, IL-17A, and TNF-α and (**G**) suppressed the decrease in IL-10 mRNA expression levels in colon samples from mice with colitis by qRT-PCR. Gene expression was normalized to β-actin in each group. (**H**) The expression of p-AKT was significantly increased in the DSS group. *$P < 0.05$, **$P < 0.01$, ***$P < 0.001$.

https://doi.org/10.2147/JIR.S516556

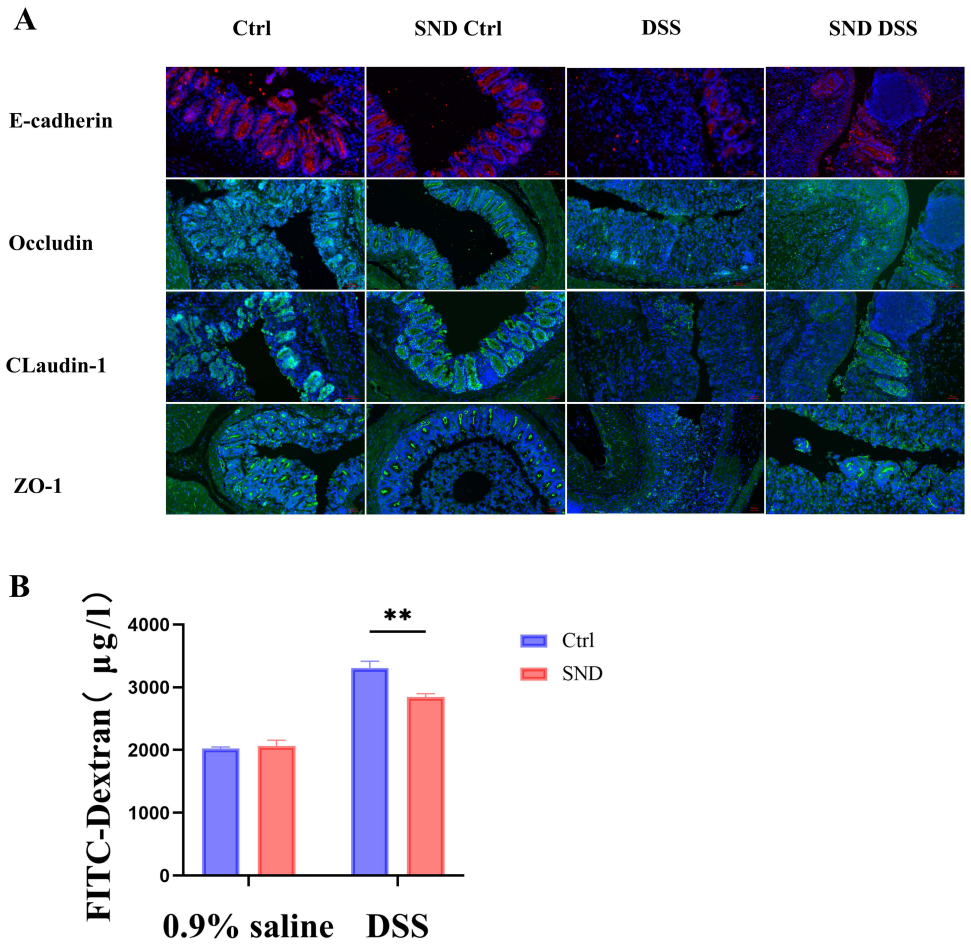

Figure 9 SND alleviates the impaired intestinal barrier associated with colitis. (**A**) The expression of tight junction proteins Occludin, E-cadherin, CLaudin-1, ZO-1 was increased in the SND DSS group compared to the DSS group. (**B**) Four groups of mice were gavage with FITC- dextrose and fluorescence levels in plasma were measured. $^{**}P < 0.01$.

following SND therapy. Histological analysis showed that DSS treatment caused a marked loss of goblet cells and crypts, pronounced edema, and neutrophil infiltration, all characteristic of UC. However, SND effectively reversed these pathological changes.[1] Overall, the anti-colitis effects of SND were apparent.

We employed network pharmacology to predict its potential targets and explore the underlying pharmacological mechanisms of Sini decoction in treating UC. By analyzing these targets, we identified pathways associated with the genes involved, including the AKT pathway and its role in responding to bacterial molecules. This suggests that Sini decoction may downregulate the AKT pathway to modulate inflammatory responses[25] and regulate the gut microbiota composition. Sustained suppression of inflammation is crucial for treating UC, as excessive immune responses can disrupt the intestinal barrier, facilitating pathogen invasion.[26] Sini decoction inhibited the mRNA expression of several inflammatory mediators in the colon and reduced protein levels of IL-1β in colonic tissue. SND treatment mitigated intestinal barrier disruption, as evidenced by increased tight junction proteins such as E-cadherin levels, compared to the DSS group.

The onset and progression of UC are associated with dysbiosis, characterized by a reduction in beneficial bacteria and an increase in harmful bacteria.[27,28] SND restored the β-diversity index in colitis mice, suggesting a rebalancing of the gut microbiota. This restoration correlated with reduced inflammatory cytokine secretion, improved intestinal barrier function, and enhanced homeostasis.[29] Herbs like licorice, epimedium, and dried ginger, which are part of SND, possess strong antibacterial properties. While they do not directly interact with sulfate, they may indirectly affect sulfate conversion by inhibiting the activity of sulfate-reducing bacteria, such as Desulfovibrionaceae, and modulating their

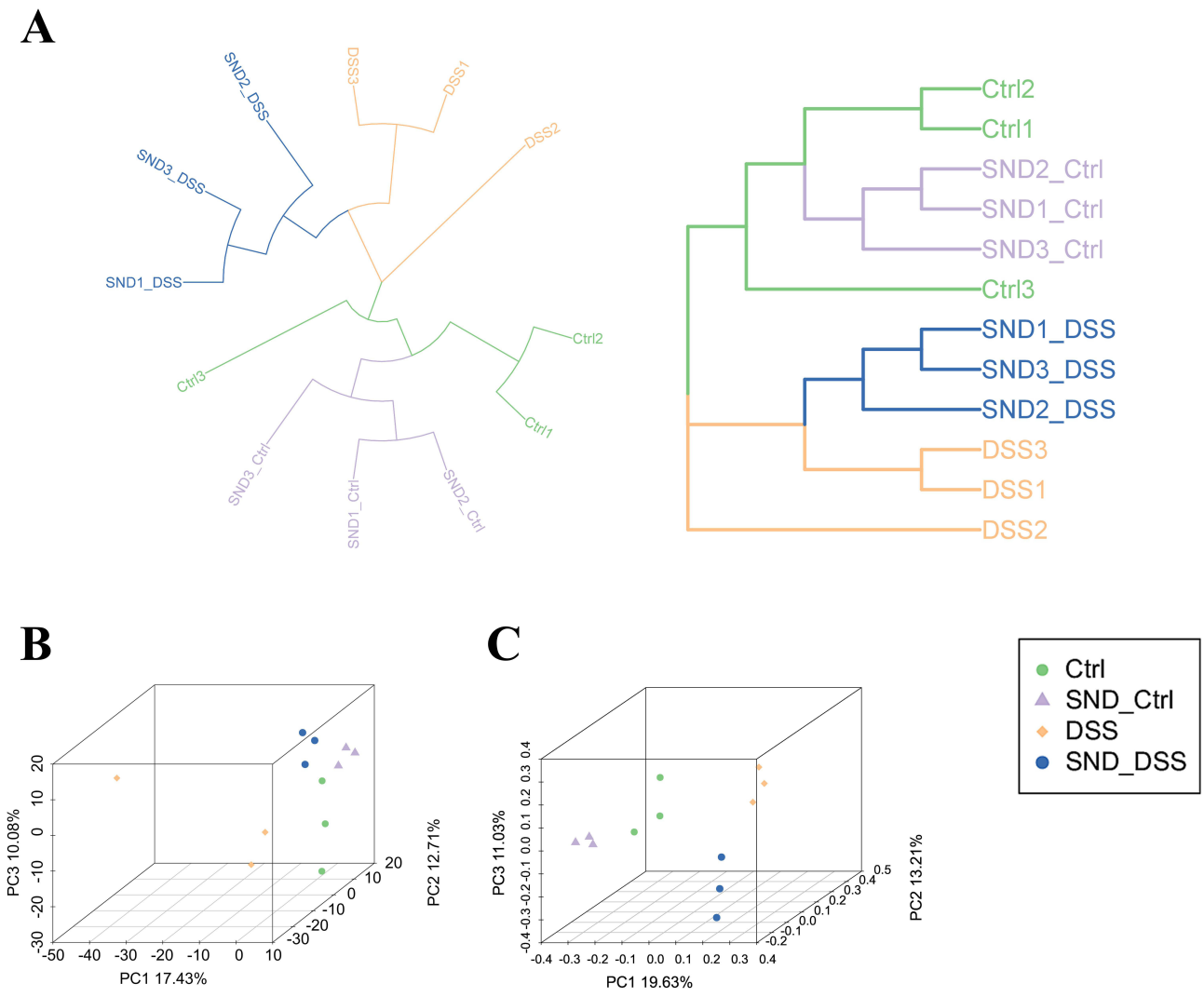

Figure 10 β-Diversity of fecal microbiota in mice. (**A**) UPGMA Sample Hierarchical Clustering Map of fecal microbiota in four groups of mice. (**B** and **C**) β-Diversity of fecal microbiota in colitis mice Represented by PCA and PcoA.

metabolic pathways.[30] The relationship between Desulfovibrionaceae, Desulfovibrionales, and Desulfobacterota follows a typical taxonomic hierarchy, representing different taxonomic levels—families, orders, and phyla, respectively. SND may alleviate intestinal inflammation by modulating the gut microbiota and inhibiting the overgrowth of harmful bacteria, such as Desulfovibrionaceae. Desulfovibrionaceae are sulfate-reducing bacteria capable of producing hydrogen sulfide, a metabolite that, at high concentrations, can be toxic to the intestinal epithelium and exacerbate inflammatory responses. The modulatory effect of SND may protect intestinal barrier function and reduce inflammation by limiting the proliferation of these harmful bacteria.

SND is also beneficial in increasing levels of beneficial bacteria such as Bacteroidota Peptococcaceae Lactobacilli, and it has been shown that these intestinal florae contribute to intestinal balance in several ways. Bacteroidota are commonly found in the human gut, where they play an important role in breaking down complex carbohydrates, producing short-chain fatty acids through fermentation of dietary fiber, which can have a positive effect on gut health. And their secretion of Sphingolipids has been shown to help regulate intestinal homeostasis.[31] Lactobacilli metabolizes tryptophan to produce indole derivatives, which act as endogenous ligands for the AHR and reduce the abundance of pathogenic bacteria.[32] In addition, Lactobacilli increases the expression of tryptophan nase and convert tryptophan to indole, which activates the AHR to repair the intestinal mucosal barrier.[33] Peptococcaceae plays an important role in the metabolism of short-chain fatty acids. Short-chain fatty acids serve as a source of energy for intestinal epithelial cells and help reduce intestinal inflammation. They

https://doi.org/10.2147/JIR.S516556

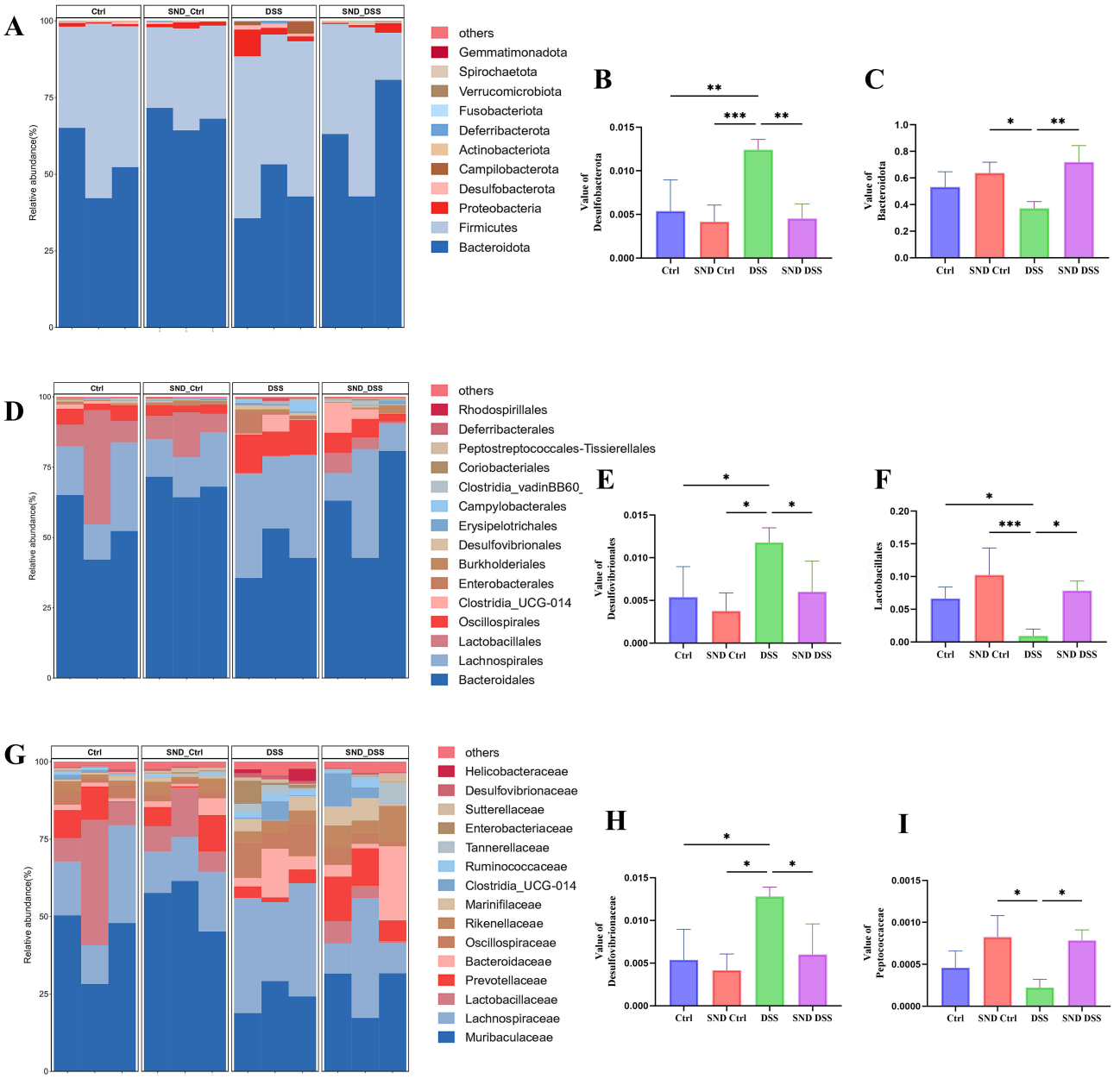

Figure 11 SND increased beneficial bacteria and decreased harmful bacteria. (**A**) A histogram of the top 15 species in terms of abundance at the phylum level. (**B**) Relative abundance values of Desulfobacterota at the phylum level.(**C**) Relative abundance values of Bacteroidota at the phylum level. (**D**) A histogram of the top 15 species in terms of abundance at the order level. (**E**) Relative abundance values of Desulfovibrionales at the order level. (**F**) Relative abundance values of Lactobacillales at the order level. (**G**) A histogram of the top 15 species in terms of abundance at the family level. (**H**) Relative abundance values of Desulfovibrionaceae at the family level. (**I**) Relative abundance values of Peptococcaceae at the family level. **P* < 0.05, ***P* < 0.01, ****P* < 0.001.

also protect the intestinal barrier function by fermenting dietary fiber and other complex carbohydrates, maintaining the microbiota balance in the gut, and inhibiting the growth of potentially pathogenic bacteria.[34,35]

Conclusion

Sini Decoction shows potential in treating ulcerative colitis by targeting key pathways. Network pharmacology revealed 193 shared targets between SND and colitis-related genes, including AKT1. In a mouse model, SND improved colon length, reduced weight loss, and alleviated histological damage. It also lowered pro-inflammatory cytokines and inhibited

the AKT pathway. SND restored intestinal barrier integrity and modulated gut microbiota by reducing harmful bacteria. These findings suggest that SND may offer a promising therapeutic approach for colitis.

Data Sharing Statement

The data that support the findings of this study are available on request from the corresponding author.

Ethical Approval Statement

This study was approved by the Scientific Research Ethics Committee of the Affiliated Hospital of Jining Medical University and the Human Research Ethics Committee (Approval No. 2021C087). All animal procedures complied with China's Regulations on the Management of Laboratory Animals, and human data research adhered to institutional and national ethical guidelines, including confidentiality protections.

Author Contributions

All authors made a significant contribution to the work reported, whether that is in the conception, study design, execution, acquisition of data, analysis and interpretation, or in all these areas; took part in drafting, revising or critically reviewing the article; gave final approval of the version to be published; have agreed on the journal to which the article has been submitted; and agree to be accountable for all aspects of the work.

Funding

This study was supported by the Taishan Young Scholars Fund of Shandong Province (tsqn202103190), the National Natural Science Foundation of China (82270562), and the Science and Technology Development Programme of Traditional Chinese Medicine of Shandong Province (M-2023173).

Disclosure

The authors declare that there are no conflicts of interest.

References

1. Ordás I, Eckmann L, Talamini M, Baumgart DC, Sandborn WJ. Ulcerative colitis. *Lancet*. 2012;380:1606–1619. doi:10.1016/s0140-6736(12)60150-0
2. Qiu P, Ishimoto T, Fu L, et al. The gut microbiota in inflammatory bowel disease. *Front Cell Infect Microbiol*. 2022;12:733992. doi:10.3389/fcimb.2022.733992
3. Khor B, Gardet A, Xavier RJ. Genetics and pathogenesis of inflammatory bowel disease. *Nature*. 2011;474:307–317. doi:10.1038/nature10209
4. Xue M, Leibovitzh H, Jingcheng S, et al. Environmental factors associated with risk of Crohn's disease development in the Crohn's and Colitis Canada - Genetic, Environmental, Microbial Project. *Clin Gastroenterol Hepatol*. 2024;22:1889–1897.e1812. doi:10.1016/j.cgh.2024.03.049
5. Voelker R. What is ulcerative colitis? *JAMA*. 2024;331:716. doi:10.1001/jama.2023.23814
6. Wangchuk P, Yeshi K, Loukas A. Ulcerative colitis: clinical biomarkers, therapeutic targets, and emerging treatments. *Trends Pharmacol Sci*. 2024;45:892–903. doi:10.1016/j.tips.2024.08.003
7. Di Sabatino A, Santacroce G, Rossi CM, Broglio G, Lenti MV. Role of mucosal immunity and epithelial-vascular barrier in modulating gut homeostasis. *Int Emerg Med*. 2023;18:1635–1646. doi:10.1007/s11739-023-03329-1
8. Turner JR. Intestinal mucosal barrier function in health and disease. *Nat Rev Immunol*. 2009;9:799–809. doi:10.1038/nri2653
9. Kayal M, Shah S. Ulcerative colitis: current and emerging treatment strategies. *J Clin Med*. 2019;9:94. doi:10.3390/jcm9010094
10. Duggal S, Jailkhani N, Midha MK, et al. Defining the Akt1 interactome and its role in regulating the cell cycle. *Sci Rep*. 2018;8:1303. doi:10.1038/s41598-018-19689-0
11. Gao J, Cao B, Zhao R, et al. Critical signaling transduction pathways and intestinal barrier: implications for pathophysiology and therapeutics. *Pharmaceuticals* 2023;16:1216. doi:10.3390/ph16091216
12. Lechuga S, Braga-Neto MB, Naydenov NG, Rieder F, Ivanov AI. Understanding disruption of the gut barrier during inflammation: should we abandon traditional epithelial cell lines and switch to intestinal organoids? *Front Immunol*. 2023;14:1108289. doi:10.3389/fimmu.2023.1108289
13. Gu Y, Li Z, Li H, et al. Exploring the efficacious constituents and underlying mechanisms of sini decoction for sepsis treatment through network pharmacology and multi-omics. *Phytomedicine*. 2024;123:155212. doi:10.1016/j.phymed.2023.155212
14. Ding X, Zhang Y, Pan P, et al. Multiple mitochondria-targeted components screened from Sini decoction improved cardiac energetics and mitochondrial dysfunction to attenuate doxorubicin-induced cardiomyopathy. *Theranostics*. 2023;13:510–530. doi:10.7150/thno.80066
15. Zhao Z, Liu J, Hu Y, et al. Bacterial diversity in the intestinal mucosa of heart failure rats treated with Sini Decoction. *BMC Complement Med Therap*. 2022;22:93. doi:10.1186/s12906-022-03575-4
16. Chen Q, Liu J, Wang W, et al. Sini decoction ameliorates sepsis-induced acute lung injury via regulating ACE2-Ang (1-7)-Mas axis and inhibiting the MAPK signaling pathway. *Biomed Pharmacother*. 2019;115:108971. doi:10.1016/j.biopha.2019.108971

17. Liang B, Liang Y, Li R, Zhang H, Gu N. Integrating systematic pharmacology-based strategy and experimental validation to explore the synergistic pharmacological mechanisms of Guanxin V in treating ventricular remodeling. *Bioorg Chem*. 2021;115:105187. doi:10.1016/j.bioorg.2021.105187
18. Szklarczyk D, Gable AL, Nastou KC, et al. The STRING database in 2021: customizable protein-protein networks, and functional characterization of user-uploaded gene/measurement sets. *Nucleic Acids Res*. 2021;49:D605–d612. doi:10.1093/nar/gkaa1074
19. Piñero J, Bravo À, Queralt-Rosinach N, et al. DisGeNET: a comprehensive platform integrating information on human disease-associated genes and variants. *Nucleic Acids Res*. 2017;45:D833–d839. doi:10.1093/nar/gkw943
20. Di H, Liu H, Xu S, Yi N, Wei G. Network pharmacology and experimental validation to explore the molecular mechanisms of compound huangbai liquid for the treatment of acne. *Drug Des Devel Ther*. 2023;17:39–53. doi:10.2147/dddt.S385208
21. Zhou Y, Zhou B, Pache L, et al. Metascape provides a biologist-oriented resource for the analysis of systems-level datasets. *Nat Commun*. 2019;10:1523. doi:10.1038/s41467-019-09234-6
22. Doncheva NT, Morris JH, Holze H, et al. Cytoscape stringApp 2.0: analysis and visualization of heterogeneous biological networks. *J Prot Res*. 2023;22:637–646. doi:10.1021/acs.jproteome.2c00651
23. Jo S, Kim T, Iyer VG, Im W. CHARMM-GUI: a web-based graphical user interface for CHARMM. *J Comput Chem*. 2008;29:1859–1865. doi:10.1002/jcc.20945
24. Mark P, Nilsson L. Structure and dynamics of the TIP3P, SPC, and SPC/E water models at 298 K. *J Phys Chem A*. 2001;105:9954–9960. doi:10.1021/jp003020w
25. Vallée A, Lecarpentier Y. Crosstalk between peroxisome proliferator-activated receptor gamma and the canonical WNT/β-catenin pathway in chronic inflammation and oxidative stress during carcinogenesis. *Front Immunol*. 2018;9:745. doi:10.3389/fimmu.2018.00745
26. Fu J, Zong X, Jin M, et al. Mechanisms and regulation of defensins in host defense. *Signal Transduct Target Ther*. 2023;8:300. doi:10.1038/s41392-023-01553-x
27. An Y, Zhai Z, Wang X, et al. Targeting Desulfovibrio vulgaris flagellin-induced NAIP/NLRC4 inflammasome activation in macrophages attenuates ulcerative colitis. *J Adv Res*. 2023;52:219–232. doi:10.1016/j.jare.2023.08.008
28. Xie R, Gu Y, Li M, et al. Desulfovibrio vulgaris interacts with novel gut epithelial immune receptor LRRC19 and exacerbates colitis. *Microbiome*. 2024;12(1):4. doi:10.1186/s40168-023-01722-8
29. Leibovitzh H, Lee S-H, Xue M, et al. Altered gut microbiome composition and function are associated with gut barrier dysfunction in healthy relatives of patients with Crohn's disease. *Gastroenterology*. 2022;163:1364–1376.e1310. doi:10.1053/j.gastro.2022.07.004
30. Lennon G, Balfe Á, Bambury N, et al. Correlations between colonic crypt mucin chemotype, inflammatory grade and DesulfovibrioD esulfovibrio species in ulcerative colitis. *Colorectal Dis*. 2014;16:O161–169. doi:10.1111/codi.12503
31. Brown EM, Ke X, Hitchcock D, et al. Bacteroides-derived sphingolipids are critical for maintaining intestinal homeostasis and symbiosis. *Cell Host Microbe*. 2019;25:668–680.e667. doi:10.1016/j.chom.2019.04.002
32. Roager HM, Licht TR. Microbial tryptophan catabolites in health and disease. *Nat Commun*. 2018;9:3294. doi:10.1038/s41467-018-05470-4
33. Agus A, Planchais J, Sokol H. Gut microbiota regulation of tryptophan metabolism in health and disease. *Cell Host Microbe*. 2018;23:716–724. doi:10.1016/j.chom.2018.05.003
34. Cao F, Pan F, Gong X, et al. Causal relationship between gut microbiota with subcutaneous and visceral adipose tissue: a bidirectional two-sample Mendelian randomization study. *Front Microbiol*. 2023;14:1285982. doi:10.3389/fmicb.2023.1285982
35. Zhang Q, Zhang Y, Zeng L, et al. The role of gut microbiota and microbiota-related serum metabolites in the progression of diabetic kidney disease. *Front Pharmacol*. 2021;12:757508. doi:10.3389/fphar.2021.757508